AIAA-2002-4261

Numerical Simulations of Ion Thruster Accelerator Grid Erosion

John R. Brophy, Ira Katz, James E. Polk, John R. Anderson
Jet Propulsion Laboratory
California Institute of Technology
Pasadena, California

The highly successful demonstration of ion propulsion on Deep Space 1 has stimulated the study of more demanding applications of ion propulsion. These future applications require ion thrusters capable of providing significantly greater specific impulses and total impulses than the current state-of-the-art. Higher specific impulses aggravate the known wear out mechanisms of the ion accelerator system. Computer simulations of the ion accelerator system operation and erosion are essential tools for the development of ion thrusters to meet the demand for higher specific impulse and longer life. Two-dimensional and three-dimensional computer codes have been developed at JPL and are used provide insight to the processes limiting the life of the accelerator grid. The 2D code was used to identify a key feature of operation at high *Isp*. That is, as the beam voltage is increased the energy of the charge-exchange ions hitting the hole walls increases in proportion to the beam voltage and more rapidly than the increase in the magnitude of the accelerator grid voltage. This has serious implications for the design of long-life, high specific impulse thrusters, and these implications are discussed herein.

Introduction

Ion propulsion is an enabling technology for many deep space missions. Future missions will require ion thrusters that operate at much higher specific impulses and for much longer durations than the NSTAR ion engine that flew successfully on Deep Space 1 [1-5]. Erosion of the accelerator grid by charge-exchange ions is one of the major failure mechanisms limiting the life of ion engines and operation at higher specific impulses (*Isp*) aggravates this erosion. Designing the ion accelerator systems to achieve long life at *Isp*'s significantly greater than 3100 s is the objective of this work.

Computer modeling is the key to cost-effectively designing advanced ion accelerator systems. We have performed two and three-dimensional numerical simulations to investigate the physics of accelerator grid erosion by charge-exchange (CEX) ions. The computer codes model ion beamlet trajectories through a single pair of screen and accelerator grid apertures in the self-consistent electric potentials found by solving Poisson's equations. The codes follow both primary ions formed inside the discharge chamber, and ions generated beyond the screen grid by charge exchange between unionized propellant atoms and primary ions.

The present investigation focuses on the key features of the physics affecting accelerator grid erosion. Charge exchange ions generated between the screen grid and the accelerator grid are subject to the strong inter grid electric field, and achieve substantial kinetic energies that are roughly proportional to the applied total voltage. Thus, the energies of these CEX ions increase as the square of the *Isp*. Some fraction of these ions hit the walls of the accelerator grid hole. They tend to hit with both substantial energy and at grazing angles causing the erosion that increases the accelerator grid hole diameters with time.

Another important parameter is the fraction of charge exchange ions created downstream of the accelerator grid that return to the grid. Our calculations show that these ions form the pits and

*Section Staff, Thermal and Propulsion Engineering Section, Member AIAA
**Technical Group Supervison, Advanced Propulsion Technology Group, Member AIAA
*Member of the Technical Staff, Advanced Propulsion Technology Group, Member AIAA

grooves pattern, and contribute little to erosion of the hole walls. Models that estimate charge exchange currents based on optical view factors are not consistent with our calculations.

Finally, we will examine the implications of these numerical simulations on the grid life expected for very high specific impulse ion engines.

Modeling Approach

CEX2D is JPL's 2-D ion optics code that includes charge exchange reactions between beam ions and un-ionized propellant gas. The code solves Poisson's equation on a regular mesh in either Cartesian or cylindrical geometry. With a few exceptions, the code uses a combination of algorithms used in previously reported ion optics codes [6-11]. Ions enter the computational region from the upstream boundary at the Bohm velocity, and their charge density is found by flowing their trajectories in a stationary electric field, as opposed to time dependent PIC simulations. The upstream electron density is found assuming a Maxwellian distribution, as compared with the sharp sheath approximation used in the OPT and IGX codes. The downstream electron population is also assumed to be a Maxwellian with a different reference potential. As a result downstream potentials are determined self consistently; there is no need to assume a neutralization plane. Charge exchange ion charge density is ignored in the calculation of potentials.

The code is written in Compaq Visual Fortran and runs under the MS Windows operating system. Potentials are calculated using an optimized pre-conditioned least square conjugate gradient sparse matrix solver from the Compaq Extended Math Library (CXML). Results for a given upstream plasma number density, n, are found by starting from zero density, and in each iteration, i, blending in a fraction, α, of the desired density.

$$n^0 = 0$$

$$n^{i+1} = (1-\alpha)n^i + \alpha n$$

If α is sufficiently small, results for all upstream densities less then n are obtained in a single run.

$$n^i = (1-(1-\alpha)^i)n$$

By saving the intermediate results, only a single run is needed to evaluate the performance of an optics design over a wide range of discharge chamber densities. A typical calculation takes tens of minutes on a newer PC.

Charge-exchange (CEX) ion generation is modeled using a Monte Carlo simulation and the trajectories of these ions are computed based on the previously calculated potential distribution. For those CEX ions that hit the accelerator grid, the code records the grid location, angle of incidence and energy of each ion.

Accelerator grid erosion is calculated using the energy-dependent sputter yield data for xenon on molybdenum given in Fig. 1 from Refs. [12-14].

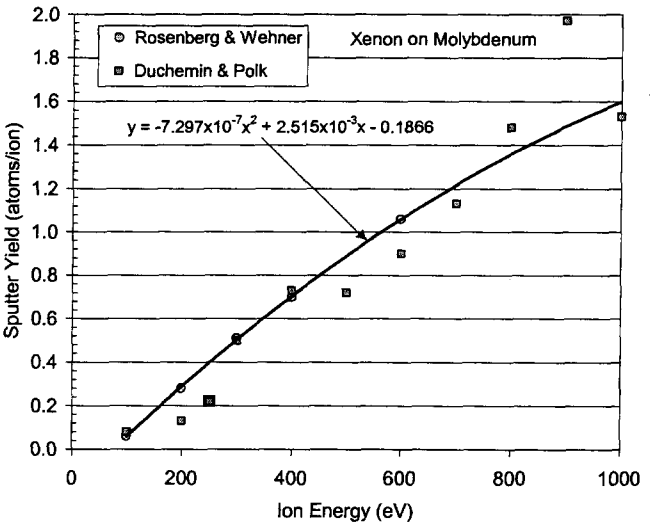

a) Ion energies < 1000 eV.

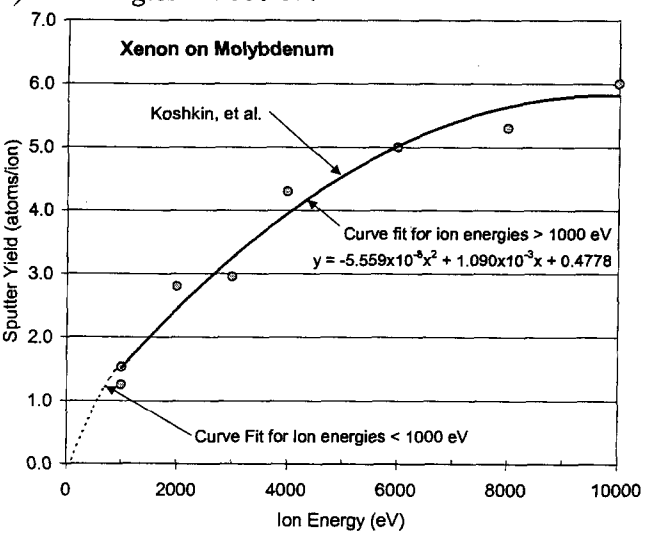

b) Ion energies > 1000 eV.

Fig. 1 Sputter yield for xenon on molybdenum for a) low energy and b) high energy.

These sputter yields are then corrected for the angle of incidence using the following relationships from Ref. [15], which are plotted in Fig. 2.

If T < 0.698 radians then,

$$Y_{corrected} = Y_0\left(1 + 0.252\theta + 0.6\theta^2 + 0.6\theta^3\right)$$

else,

$$Y_{corrected} = Y_0\left[-0.057 + 1.9\exp\left(-\left(\frac{\theta - 0.8201}{0.401}\right)^2\right)\right]$$

This angular sputter yield data was measured at a xenon ion energy of 350 eV, but we have used this same angular dependence at all ion energies.

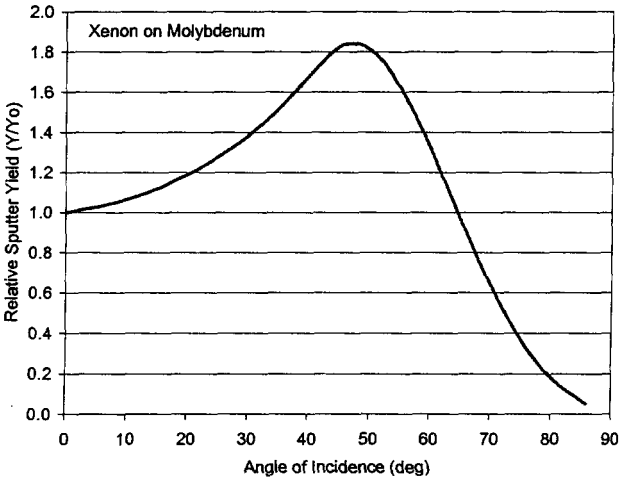

Fig. 2 Angular dependence of the sputter yield for xenon on molybdenum at 350 eV.

Code Validation

Several tests of the CEX2D code were performed to validate it against existing data. There is extensive accelerator grid erosion data available from the life tests performed under the NSTAR program on NASA's 30-cm diameter thruster [16-19]. Therefore, several comparisons with these data were made. In addition, the ability of the code to predict the perveance and cross over limits for grids operating at specific impulses greater than 7000 s were compared with experimental data. For the discussions that follows the conventional nomenclature, as defined in Fig. 2, is used.

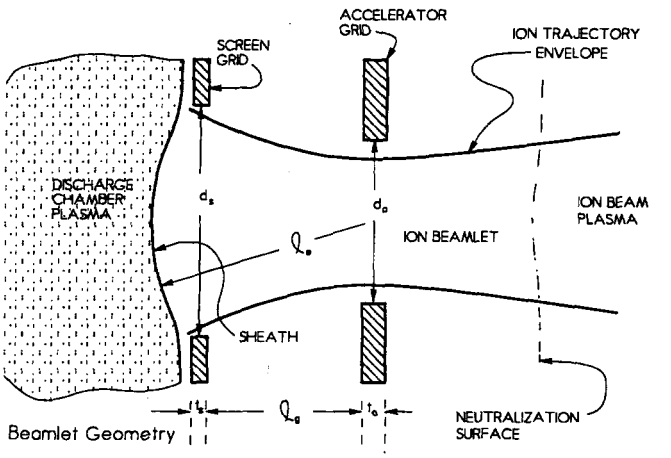

Fig. 3 Grid geometry definitions (figure courtesy of Paul Wilbur at Colorado State University).

Comparison with NSTAR Life Test Data

Screen Grid Transparency. The screen grid transparency to ions, ϕ_i, has been measured for the NSTAR thruster as a function of throttle level several life tests. The CEX2D code was used to calculate the expected screen grid transparency at beginning-of-life (BOL) to compare to these data. The measured values of ϕ_i, however, are a measure of the effective transparency over the entire grid. The CEX2D code examines only a single pair of screen and accelerator grid apertures. As mentioned above, the code provides information regarding the grid performance over a wide range of plasma densities in a single run. These data were used together with the known radial variation in beam current density of the NSTAR thruster to determine the radial variation in ϕ_i. The average value of ϕ_i was then calculated by integrating over the grid surface, i.e.,

$$\bar{\phi}_i = \frac{\int j_b \phi_i dr}{\int j_b dr} \qquad (1)$$

The resulting values are shown in Fig. 3 and compare well with the measured screen grid transparencies from the beginning of the Extended Life Test (ELT) Ref [19].

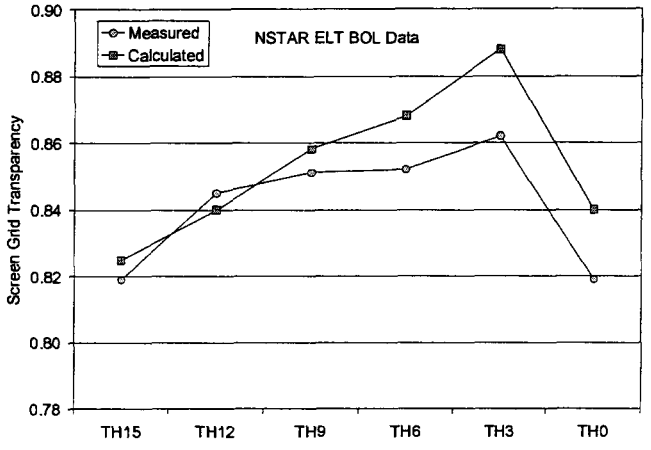

Fig. 3 The CEX2D code predictions for the screen grid transparency agree reasonably well with the beginning of life NSTAR measurements as a function of throttle level.

Electron-Backstreaming. In the ELT, the accelerator grid voltage at which electron-backstreaming occurs is measured at regular intervals throughout the test. In addition, the diameter of selected accelerator grid apertures, including the center aperture, is measured at regular intervals. This makes it possible to plot the electron-backstreaming voltage as a function of accelerator aperture diameter as shown in Fig. 4 (for operation at the full power throttle level, TH15). Also shown in this figure are the values of the electron-backstreaming voltage calculated with the CEX2D code. The code predicts electron-backstreaming at more negative values than measured for a given d_a, but gives the same slope for changes in d_a.

Accelerator Grid Aperture Erosion. After the 8,200-hr NSTAR Life Demonstration Test (LDT) the diameters of the accelerator grid apertures were measured as a function of grid radius [18]. These data are given in Fig. 5. Also shown in this figure are the hole diameters calculated using the CEX2D code. To obtain these results the code was used to calculate the erosion rate of the accelerator grid hole wall for over a range of beamlet current densities. Each beamlet current density corresponds to a particular radial location on the grid. The calculated hole wall erosion rates were assumed to be constant with time allowing the hole diameters corresponding to the LDT end-of-test conditions to be calculated. To determine the final hole diameters it was assumed that the erosion first removed the cusps and then eroded the aperture walls uniformly over the thickness of the grid. The calculated hole diameters agree well with the measured values in the center of the grid, but over-predict the diameters at the periphery.

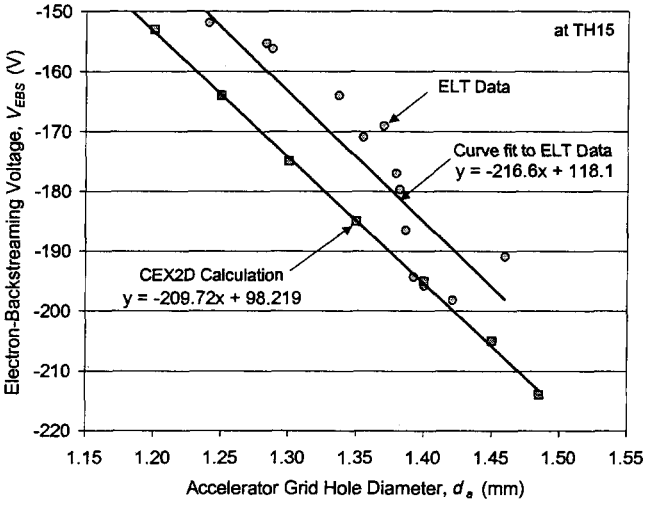

Fig. 4 The CEX2D calculated variation in electron-backstreaming voltage with increasing accelerator grid aperture diameter agrees well with the measured variation from the NSTAR ELT.

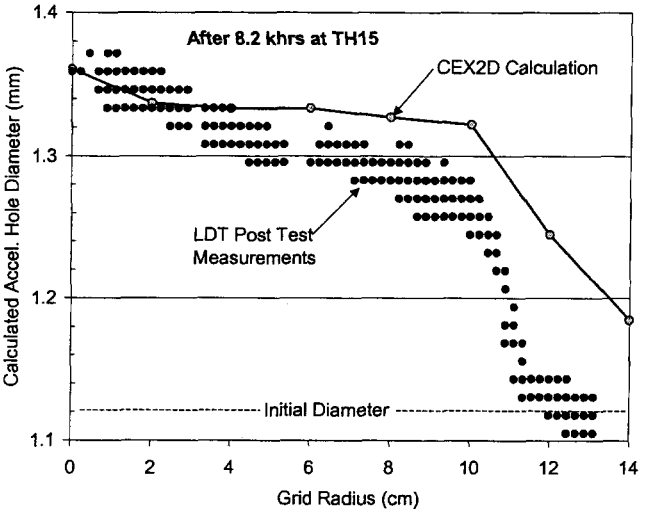

Fig. 5 Calculated accelerator grid hole diameters using the CEX2D code agree well with the values measured after the NSTAR Life Demonstration Test.

Long-Life Grids for High *Isp* Operation

The objective for the design of a new ion accelerator system is to maximize its service life for a given specific impulse and plasma density profile. This task becomes more difficult the higher the desired value of *Isp*. The beam voltage varies as the square of the *Isp*, i.e.,

$$V_B = \frac{(\eta_u \alpha F_T)^2}{2e} I_{sp}^2 \qquad (2)$$

so that higher *Isp*'s require significant increases in beam voltage.

Electron-Backstreaming (EBS) Considerations

Higher beam voltages require more negative accelerator grid voltages to prevent electron backstreaming. The maximum net-to-total voltage ratio defined as,

$$R_{max} = V_B/(V_B+|V_a|)\,, \qquad (3)$$

where |Va| is the accelerator voltage at the onset of electron-backstreamng. Kaufman [20] gives R_{max} as,

$$R_{\max} = 1 = \frac{1}{2\pi}\left(\frac{d_a}{l_e}\right) e^{-t_a/d_a} \qquad (4)$$

where,

$$l_e = \sqrt{\left(l_g + t_s\right)^2 + \frac{1}{4} d_s^2}\quad . \qquad (5)$$

Combining Eqs. (3) and (4) yields the value for $|V_a|$ at electron-backstreaming,

$$|V_a| = \frac{V_B}{2\pi \frac{l_e}{d_a} \exp\left(\frac{t_a}{d_a}\right) - 1}\,. \qquad (6)$$

Equation (6) gives the magnitude of the accelerator grid voltage at EBS as a function of the geometry of the grids. Calculated values of |Va| at EBS are compared to measured values from Wilbur [21] in Fig. 6.

Equation (6) can be used to provide guidance to the relative effects of grid geometry changes on the accelerator grid voltage required to prevent electron backstreaming. For example the accelerator grid voltage at EBS is plotted as a function of beam voltage in Fig. 7 for three different values of the ratio *lg/ds*. It is clear from this figure that operation that larger *le/ds* is desirable to minimize $|V_a|$. It is also known that larger values of *le/ds* generally result in smaller beam divergence angles [22].

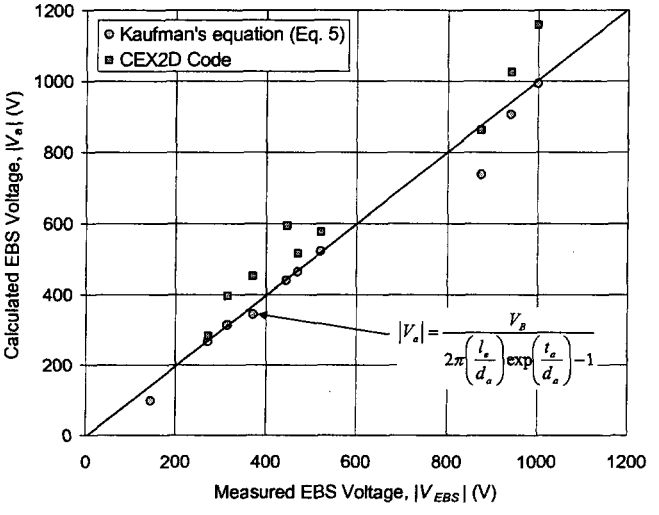

Fig. 6 Calculated values for the accelerator grid voltage at the onset of electron-backstreaming from Eq. (6) agree well with measured values. The CEX2D code also predicts the correct trend, but tends to over-predict the value of $|V_a|$ at EBS.

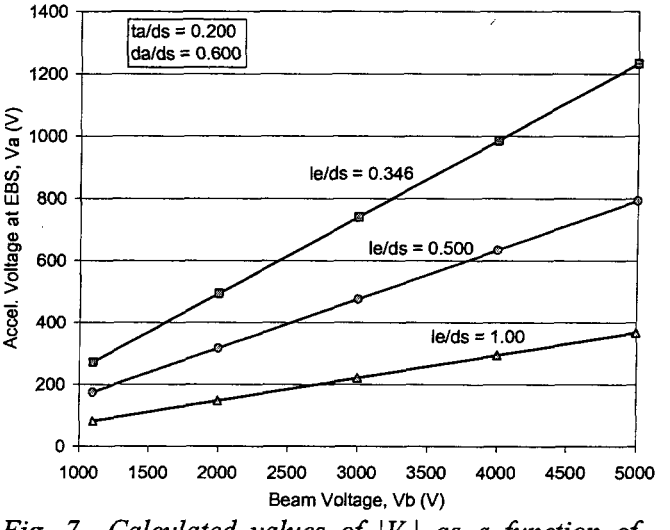

Fig. 7 Calculated values of $|V_a|$ as a function of beam voltage from Eq. (6) indicate that increasing le/ds minimizes $|V_a|$.

Accelerator Grid Hole Wall Erosion

Increasing the beam voltage increases the energy of the charge-exchange (CEX) ions that strike the walls of the accelerator grid holes. The 2D code was used to determine the average energy of the CEX ions hitting the accelerator hole wall as a function of beam

voltage for operation at approximately 75% of the theoretical maximum perveance. The results are given in Fig. 8 indicating a linear relationship between the hole wall CEX ion energy and the beam voltage. This occurs because at this perveance level, many of the CEX ions that strike the hole walls originate in the region between the screen and accelerator grids, and therefore, acquire an energy that is a function of the beam voltage. In these calculations the accelerator grid voltage was set at 25% greater than the value calculated from Eq. (6) for each beam voltage.

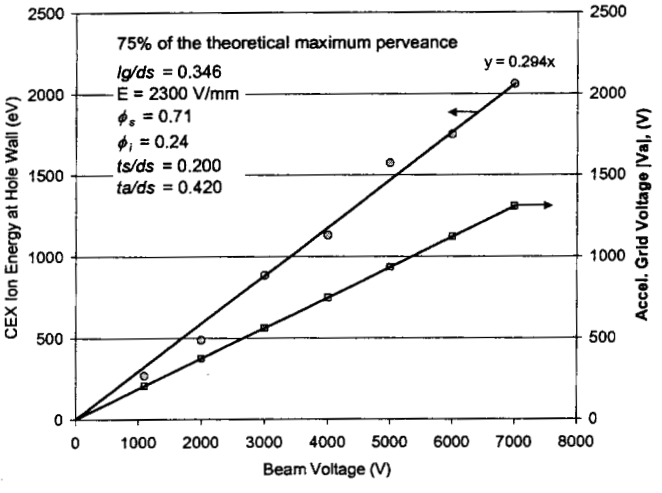

Fig. 8 The average energy of the CEX ions hitting the accelerator grid hole wall, for lg/ds = 0.346 increases linearly with beam voltage and is greater than the magnitude of the voltage applied to the accelerator grid for operation at 75 % of the theoretical maximum Perveance.

At the higher value of *le/ds* = 1.00, the increase in $|V_a|$ with V_B is smaller, as was shown in Fig. 8, but the energy of the CEX ions hitting the accelerator hole walls follows the same increase with V_B as it did with *le/ds* = 0.346. This case is given in Fig. 9, and shows a much larger difference between the CEX ion energy and the magnitude of the accelerator grid voltage. Note that the data in Fig. 9 were calculated at 67% of the theoretical maximum perveance, whereas the data in Fig. 8 were calculated at 75% of the maximum perveance. It is clear from these figures that the energy of the CEX ions hitting the hole walls is not a significant function of the *lg/ds*. This, as we shall see later, is true only if the accelerator system is operating at more than roughly 35% of the theoretical maximum perveance.

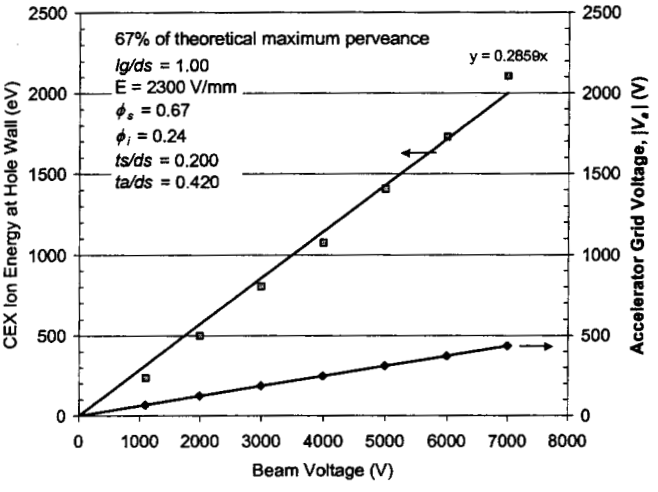

Fig. 9 The average energy of the CEX ion hitting the accelerator hole wall for lg/ds = 1.00 is the same function of V_B as it was for lg/ds = 0.346.

Since V_B varies as the square of the *Isp*, the average energy of the CEX ions hitting the hole walls also increases as the square of the *Isp* so that long-life operation at high *Isp* becomes increasingly more difficult.

CEX Ion Production

The location of CEX ion production is illustrated in Fig. 10. CEX ions created in the shaded region will strike the walls of the accelerator grid apertures, and will do so with an energy proportional to the beam voltage. The CEX ions that are produced in the central region of the beamlet get focused out through the accelerator grid aperture and cause no grid erosion. If the beamlet can be focused entirely within the indicated central region, then the erosion of the accelerator grid hole wall will be greatly reduced. To do this, as we will show later, requires operation at a small fraction of the theoretical maximum perveance. Such operation results in beamlets with sufficiently small diameters that all of the CEX ions created between the grids get focused out through the accelerator grid apertures.

The current density of CEX ions produced between the grids may be approximated as,

$$j_{CEX} = \sigma_{CEX} n_0 l_e j_b \quad . \tag{7}$$

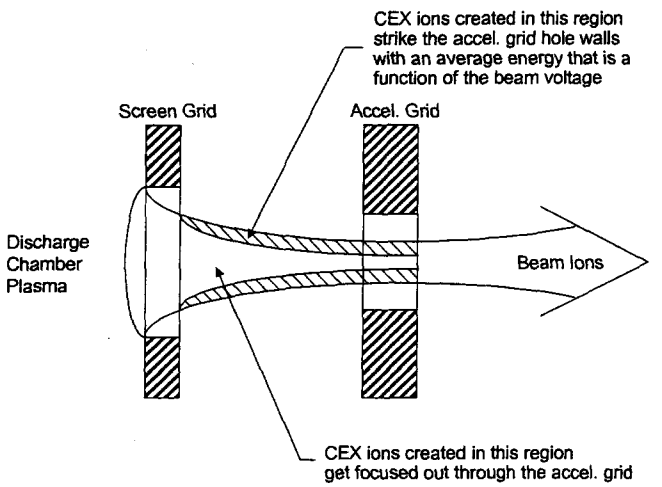

Fig. 10 The location of CEX ion production affects where these ions go and how much energy they acquire.

Assuming free molecular flow, the density of neutral atoms in the discharge chamber, n_0, may be approximated by,

$$n_0 = \frac{4\dot{m}_d(1-\eta_{ud})}{m_i v_0 A_g \phi_a} , \qquad (8)$$

where the discharge chamber propellant efficiency is,

$$\eta_{ud} = \frac{J_B}{\dot{m}_d}\left(\frac{m_i}{e}\right) , \qquad (8)$$

and the beam current is given by,

$$J_B = j_b f_b A_g . \qquad (9)$$

Combining Eqs. (7) through (9) yields,

$$j_{CEX} = l_e j_b^2 \frac{4\sigma_{CEX} f_b}{v_0 \phi_a e}\left(\frac{1-\eta_{ud}}{\eta_{ud}}\right) . \qquad (10)$$

Finally, if we approximate l_e by l_g, then we can replace l_g with V_T/E to get,

$$j_{CEX} \propto j_b^2 \frac{V_T}{E}\left(\frac{1-\eta_{ud}}{\eta_{ud}}\right) . \qquad (11)$$

This equation indicates that the CEX ion current density increases as the square of the beam current density, linearly with the total voltage, and decreases with increasing electric field.

While not all of the CEX ions produced between the grids will hit the accelerator grid, it is clearly desirable to minimize the production of these ions. Therefore, for a given beam current density and total voltage, Eq. (11) suggests that the ion accelerator system should be operated at the maximum possible electric field. Maximizing the electric field, minimizes the distance between the grids for the production of CEX ions for a given total voltage.

From Eq. (6) we concluded that it was desirable to operate with large values of *le/ds*. Equation (11) indicates that it is also desirable to operate with the maximum possible electric field to minimize the l_g (which also minimizes l_e). The only way to have a large value for *le/ds* while minimizing l_e is to have very small diameter screen grid holes. For fixed ratios *ts/ds*, and *ta/ds*, very small d_s will result in very thin grids. The screen grid hole size, therefore, must be selected such that the grids can be manufactured and proper alignment between the screen and accelerator grid apertures can be achieved.

Behavior of the CEX Ions

Computer simulations provide a wealth of information regarding the behavior of the CEX ions including the location where every CEX ion is created, where it goes, and for those ions that hit the accelerator grid, what angle and energy they have. This capability enables the problem of the accelerator grid hole wall erosion to be separated from the erosion on the downstream side of the grid.

CEX Ions that Hit the Hole Walls

The average energy of the CEX ions that hit the accelerator grid hole wall is a function of the perveance. Child's law gives an expression for the current density, j_b, between the grids,

$$j_b = \frac{4\pi}{9}\left(\frac{2e}{m_i}\right)^{1/2}\frac{V_T^{3/2}}{l_e^2} , \qquad (12)$$

where,

$$V_T = V_B + V_a . \qquad (13)$$

The perveance, P, is defined from this equation as,

$$P = \frac{j_b l_e^2}{V_T^{3/2}} , \qquad (14)$$

and the theoretical maximum perveance is [22],

$$P_{max} = \frac{4\pi}{9}\left(\frac{2e}{m_i}\right)^{1/2} \qquad (15)$$

For Xe with a mass of $m_i = 2.18\text{x}10^{-25}$ kg, the theoretical maximum perveance is,

$$P_{max} = 4.77\text{x}10^{-9}\ \text{A/V}^{3/2}$$

Real ion accelerator systems always operate at a fraction, f_p, of this theoretical maximum perveance, i.e.,

$$\frac{j_b l_e^2}{V_T^{3/2}} = f_p P_{\max} \quad . \qquad (16)$$

For example, the NSTAR ion thruster operating at full power (TH15) produces a peak beam current density of 61 A/m^2. Dividing this by the effective transparency of the screen grid (~0.82) results in the peak beam current density at the beamlet sheath of 74 A/m^2. For the NSTAR grid geometry, $l_e = 1.41\text{x}10^{-3}$ m (assuming l_g is the cold grid gap), and at full power $V_T = 1280$ V, so that $f_p = 0.67$. That is, at full power the NSTAR grids are operating at 67% of the theoretical maximum perveance.

The average energy of the CEX ions hitting the accelerator hole walls calculated using the 2D code is given in Fig. 11 as a function of f_p for *lg/ds* = 0.346. These data indicate that there is an optimum value for the fraction of the maximum perveance that minimizes the energy of the CEX ions that hit the accelerator hole walls. Furthermore, this fraction is relatively small, roughly only 20% of the theoretical maximum. Operation at 67% of the theoretical maximum, as the NSTAR thruster does at full power, results in much more energetic CEX ions hitting the hole walls for operation at high *Isp* and more rapid enlargement of the accelerator grid apertures.

The explanation for this behavior is illustrated in Fig. 12 which shows the locations where CEX ions are formed the subsequently hit the walls of the accelerator grid as a function of the perveance fraction. As the perveance fraction decreases toward the optimum, fewer CEX ions that hit the hole walls are created in the region between the grids. Only CEX ions created between the grids can obtain energies proportional to the beam voltage, so eliminating these ions significantly reduces the average energy of the CEX ions hitting the hole walls.

The optimum value for f_p is a function of *lg/ds* as indicated in Fig. 13. These data indicate that larger values of *lg/ds* result in larger values for the optimum f_p. Larger values for f_p are desirable because they enable operation at higher beam current densities while still minimizing the energy of the CEX ions hitting the accel. hole walls.

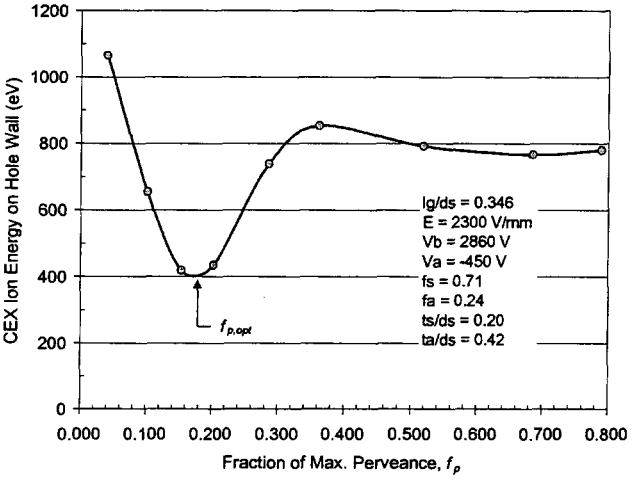

Fig. 11 There is an optimum value for f_p that minimizes the average CEX ion energy hitting the accel. hole walls.

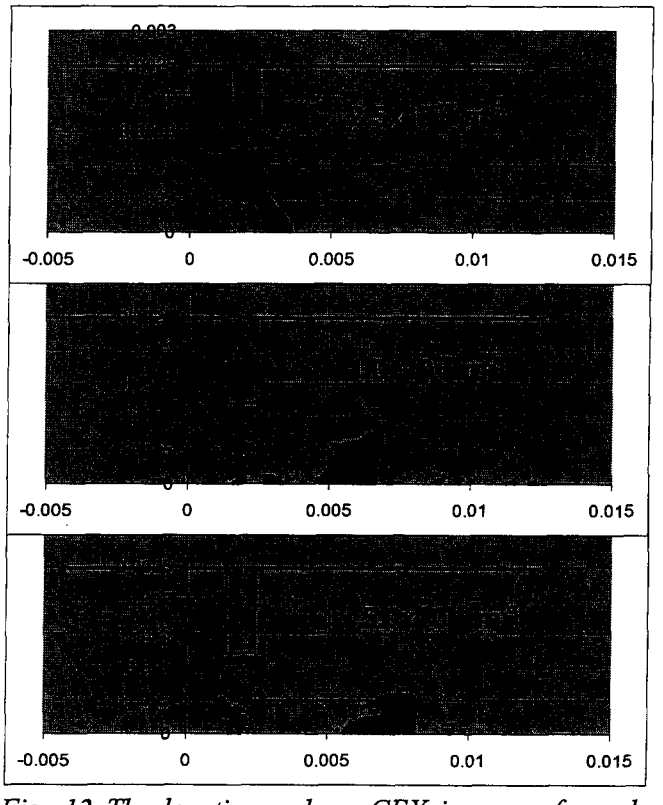

Fig. 12 The locations where CEX ions are formed that hit the accelerator grid hole walls depends on the perveance fraction.

To maximize the service life of the accelerator grid it is necessary to design the accelerator system to operate at $f_{p,opt}$ at the peak plasma density. Figure 14 shows that the energy of the CEX ions hitting the

accelerator hole walls increases much more slowly with beam voltage for operation at $f_{p,opt}$.

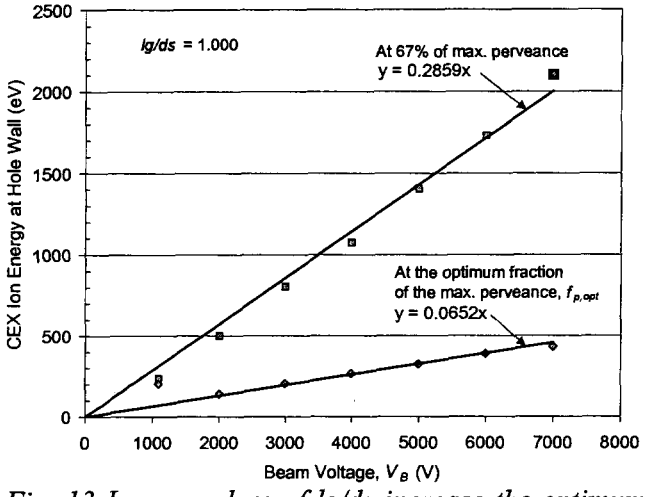

Fig. 13 Larger values of lg/ds increase the optimum fraction of the maximum perveance.

This, however, has two problems. First, the optimum is a small fraction of the theoretical maximum perveance. This constraint will result in larger thruster diameters in order to extract the desired beam current. Second, operation at the optimum perveance fraction at the peak plasma density will result in operation at much smaller perveance fractions as the plasma density decreases away from the peak. The optimum perveance fraction is so low that it leaves little "room" to accommodate the lower plasma densities before the onset of over-focusing and direct impingement due to cross-over ion trajectories.

One approach to accommodating this problem is to operate to the right of the optimum perveance fraction at the peak plasma density and accept the higher CEX ion energies at the hole walls. This is the approach the NSTAR ion accelerator system uses in which the grids operate at 67% of the maximum perveance at the peak plasma density. This is well to the right of the optimum and enables the accelerator system to accommodate a large variation in plasma densities upstream of the grids. The NSTAR ion optics must accommodate a 10-to-1 variation in plasma density from the centerline to the edge of the grids at full power. In addition, the NSTAR thruster is throttled at constant *Isp* which requires the grid system to operate over even a larger variation in plasma densities with the same grid voltages.

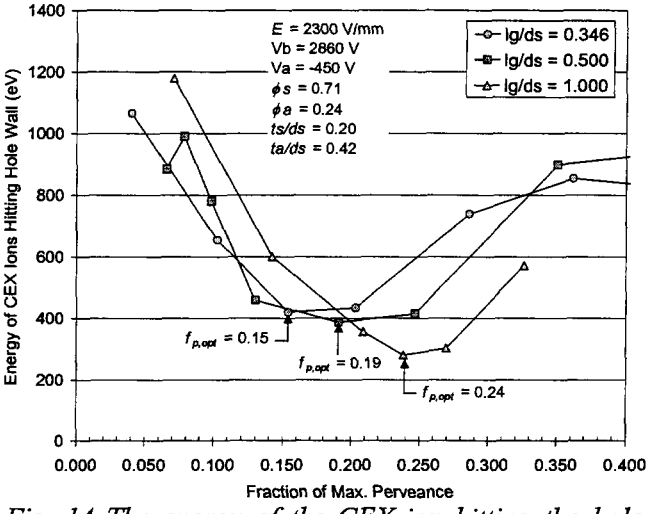

Fig. 14 The energy of the CEX ion hitting the hole walls increases much more slowly with V_B when the grids are operated at the optimum fraction of the theoretical maximum perveance.

Operation with $f_p = 0.67$ at full power at the peak plasma density is OK for the NSTAR accelerator system because the beam voltage is relatively low resulting in acceptable erosion of the accelerator grid apertures. However, for ion thrusters designed to operate at much higher *Isp*'s it will be necessary to operate closer to the optimum f_p at the peak plasma density in order to achieve adequate grid life.

A discharge chamber that produces a smaller ratio of maximum-to-minimum plasma densities enables operation of the grid system closer to the optimum perveance fraction across the accelerator system as illustrated in Fig. 15.

The minimum erosion of the accelerator grid is achieved when the accelerator system is configured to operate locally at the optimum perveance fraction everywhere on the grid. Because the plasma density varies across the grid, the only way to operate at a fixed fraction of the maximum theoretical perveance is to vary l_e with the plasma density. Solving Eq. (16) for l_e gives,

$$l_e^2 = f_{p,opt} P_{\max} \frac{V_T^{3/2}}{j_b} . \qquad (17)$$

But, l_e depends on l_g, t_s, and d_s according to Eq. (5). For a fixed total voltage, V_T, and a fixed value of $f_{p,opt}$, Eq. (17) indicates that l_e^2 must increase as the beam current density (i.e., plasma density) decreases. It is inconvenient to increase d_s as a function of radius across the grid. Therefore, we can increase either the screen grid thickness, t_s, or the grid gap, l_g, or both.

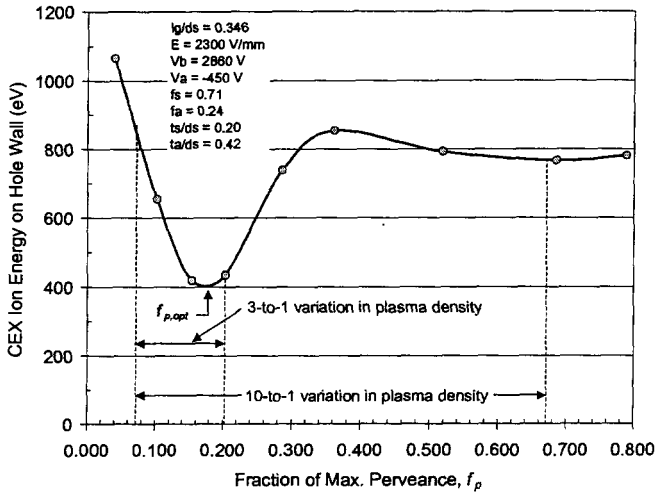

Fig. 15 Smaller ratios of the maximum to minimum plasma densities upstream of the grids enables operation closer to the optimum perveance fraction at the peak plasma density.

Screen Grid Transparency

The screen grid transparency is a function of *ts/ds* so that we cannot arbitrarily increase t_s. The variation of the screen grid transparency to ions, ϕ_I, is given as a function of *ts/ds* in Fig. 16.

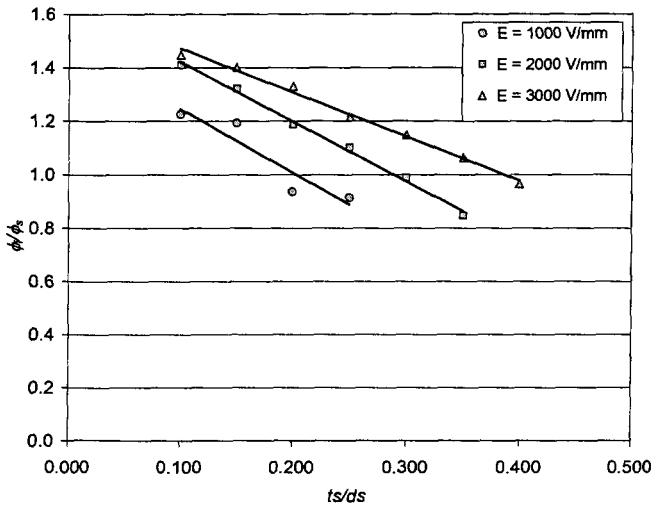

Fig. 16 Screen grid transparency to ions is a function of the screen grid thickness to screen grid hole diameter ratio.

A curve fit to the data in Fig. 14 provides the following expression for the ratio of the screen grid transparency to its physical open area fraction as a function of *ts/ds*. This equation allows the screen grid thickness to be calculated for a desired value of the screen grid transparency and given values of the physical open area fraction and the screen grid hole diameter.

$$\frac{\phi_i}{\phi_s} = f(t_s / d_s) \ . \qquad (18)$$

Grid Gap

Equation (17) can be solved for the ratio *lg/ds*, i.e.,

$$\frac{l_g}{d_s} = -\frac{t_s}{d_s} + \sqrt{f_{p,opt} P_{\max} \frac{V_T^{3/2}}{d_s^2 j_b} - \frac{1}{4}} \ . \qquad (19)$$

This equation gives the value of *lg/ds* that results in local operation of the ion accelerator system at the optimum fraction of the maximum theoretical perveance for the local beam current density, j_b, where *ts/ds* is given by Eq. (18). It is clear from Eq. (19) that for a fixed screen grid hole diameter, d_s, the grid gap, l_g, must increase as the local beam current density decreases.

Operation at or near $f_{p,opt}$ minimizes the diameters of the beamlets as they pass through the accelerator grid. Minimizing the beamlet diameters will enable the diameter of the accelerator grid apertures to also be minimized. Thus, the accelerator grid hole diameters could be tailored to follow the radial variation in beamlet diameters across the accelerator system. At the periphery of the accelerator system, where the local beam current density is expected to be low, the accelerator grid apertures could be made smaller to reduce the open area fraction of the grid, provided the grid gap is adjusted to prevent beamlet spreading due to cross over ion trajectories. Reduction of the accelerator grid open area fraction will improve the thruster propellant efficiency, potentially enable lower discharge voltage operation for lighter propellant gases and improve the overall thruster efficiency.

To follow this approach requires fabrication techniques that enable the screen and accelerator grids to have different curvatures. This should be readily achievable in the fabrication of carbon grids.

Screen Grid Hole Diameter

In order to use Eq. (19) to calculate the radial variation in screen grid thickness and grid gap we must know the screen grid hole diameter, d_s. The

diameter of the screen grid holes is obtained by substituting Eq. (5) into Eq. (17) and solving for d_s, to get,

$$d_s = \sqrt{f_{p,opt} P_{\max} \frac{V_T^{3/2}}{j_b} - \left(\frac{V_T}{E} + t_s\right)^2} \quad . \qquad (20)$$

where we have used $l_g = V_T/E$. To use Eq. (20) to calculate d_s, we select the desired value for the ratio *ts/ds* and the electric field, E. For a given V_B, j_b, and $f_{p,opt}$, Eqs. (5, 6, 13 and 19) are then solved iteratively to determine d_s, t_s, and l_g, where j_b is assumed to be the maximum expected value. An actual grid design would add some margin to the determination of $|V_a|$ in Eq. (6) either in the form of a fixed additional voltage or a percentage increase. Once d_s and l_g are known at the center of the grids, the variation in grid gap with radius may be calculated from Eq. (19).

CEX Ions that Hits the Downstream Surface

Erosion on the downstream side of the accelerator grid for the NSTAR thruster has been modeled to a high degree of fidelity by Wang, et al. [ref.]. As the *Isp* is increased this erosion phenomena also becomes more important. To see this, we follow the process outlined above to determine d_s and we hold *ta/ds* constant. It appears that in all cases the magnitude of the accelerator grid voltage increases faster than the thickness of the accelerator grid. However, the process described above to operate at $f_{p,opt}$, which is a small fraction of the maximum perveance, will also reduce the erosion on the downstream side of the accelerator grid. This is because the reduced beam current density will result in a reduced current density of CEX ions produced downstream of the accelerator grid.

Conclusions

Computer modeling is essential for the design of long-life, high-*Isp* grids, and should enable a significant reduction in cut-and-try development. Understanding the physics of the grid wearout processes is crucial to establish the grid service life since the desired lifetimes are so long.

Above a certain perveance level, the energy of the CEX ions hitting the accelerator grid hole walls increases approximately linearly with beam voltage, and hence, quadratically with *Isp*. Long accelerator grid life can only be achieved for perveance levels below this. There is an optimum value for the perveance, which we define in terms of the fraction of the maximum theoretical perveance, that minimizes the energy of the CEX ions hitting the hole walls. This optimum is a small fraction, in the range of 15% to 25%, of the theoretical maximum perveance, and implies the necessity for large diameter thrusters to provide long grid life at high *Isp*. The use of erosion resistant grid materials, such as carbon, can be used to produce smaller diameter thrusters, or extend grid life.

Low centerline perveance values (high perveance margins on the centerline) make cross over impingement more likely at the outer edges of the grid and place restrictions on the maximum to minimum density range. Grid designs that vary the screen grid thickness and grid gap to follow the radial variation in plasma density can significantly improve the range of plasma densities the accelerator system can accommodate. New grid fabrication processes are required to enable this capability. The fabrication processes used for carbon grids appear to be readily adaptable to providing this capability.

Control of the beamlet diameters at the accelerator grid can enable tailoring of the accelerator grid apertures to follow the size of the beamlets. This could enable the development of accelerator grids that have lower overall open area fractions, but can still extract the desired beam current densities across the grids. Lower open area fraction accelerator grids can improve the thruster propellant efficiency and the overall thruster efficiency.

Acknowledgements

The authors thank Dr. Paul Wilbur at Colorado State University for helpful discussions and timely testing of candidate "gridlets" designs. The work described in this paper was conducted, in part, by the Jet Propulsion Laboratory, California Institute of Technology, under contract to the National Aeronautics and Space Administration.

References

1. M. D. Rayman, P. Varghese, D. H. Lehman, and L. L. Livesay, "Results From The Deep Space 1 Technology Validation Mission," IAA-99-IAA.11.2.01, Presented at the 50th International Astronautical Congress, Amsterdam, The

Netherlands, 4-8 October, 1999, Acta Astronautica 47, p. 475 (2000).
2. M. D. Rayman and P. Varghese, "The Deep Space 1 Extended Mission," Acta Astronautica 48, No. 5-12, pp. 693-705 (2001).
3. J. E. Polk, et al., "Demonstration of the NSTAR Ion Propulsion System on the Deep Space One Mission," IEPC-01-075, Presented at the 27th International Electric Propulsion Conference, Pasadena, CA, 15-19 October, 2001.
4. J. E. Polk, et al., "Performance of the NSTAR Ion Propulsion System on the Deep Space One Mission," AIAA 2001-0965, presented at the 39th AIAA Aerospace Sciences Meeting & Exhibit, 8-11 January 2001, Reno, NV.
5. J. Brophy, et al., "The DS1 Hyper-Extended Mission, AIAA-2002-3673, to be presented at the 38th AIAA/ASME/SAE/ASEE Joint Propulsion Conference & Exhibit, Indianapolis, Indiana, 7 - 10 Jul 2002.
6. Y. Arakawa and M. Nakano, *An efficient three-dimensional optics code for ion thruster research*, AIAA 96-3198
7. M. Nakano and Y. Arakawa, *Ion Thruster Lifetime Estimation and Modeling Using Computer Simulation* IEPC 99-145
8. Y. Nakayama and P. Wilbur, *Numerical Simulation of Ion Beam Optics for Many-Grid Systems* JPC 2001
9. I. Boyd & M. Crofton, *Grid Erosion Analysis of The T5 Ion Thruster* AIAA-2001-3781
10. Y. Okawa et. al., *Numerical Analysis of Ion Beam Extraction Phenomena in an Ion Thruster* IEPC 01-97
11. J. Wang et. al., *Three-Dimensional Particle Simulations of NSTAR Ion Optics* IEPC 01-85
12. Rosenberg, D. and Wehner, G.K., "Sputtering Yields for Low Energy He+-, Kr+-, and Xe+- Ion Bombardment," Journal of Applied Physics, Vol. 33, No. 5, 1842-1845, May 1962.
13. Duchemin & Polk
14. Big Book of Sputtering
15. Jay's ref. on angular dependence of sputtering
16. M.J. Patterson, V.K. Rawlin, and J.S. Sovey, "2.3 kW Ion Thruster Wear Test," AIAA-95-2516, presented at the 31St Joint Propulsion Conference, San Diego, CA, 1995.
17. J.E. Polk, et al., "A lOOO-Hour Wear Test of the NASA NSTAR Ion Thruster," AIAA-96-2717, presented at the 32nd Joint Propulsion Conference, Lake Buena Vista, FL, 1996.
18. J. E. Polk, et al., "An Overview of the Results from an 8200 Hour Wear Test of the NSTAR Ion Thruster," AIAA 99-2446, presented at the 35th AIAA/ASME/SAE/ASEE Joint Propulsion Conference and Exhibit, 20-24 June 1999, Los Angeles, California
19. A. Sengupta, et al., "Performance Characteristics of the Deep Space 1 Flight Spare Ion Thruster Long Duration Test after 21,300 Hours of Operation," AIAA-2002-3959, to be presented at the 38th AIAA/ASME/SAE/ASEE Joint Propulsion Conference & Exhibit, Indianapolis, Indiana, 7 - 10 Jul 2002.
20. H. Haufman, "Technology of Electron-Bombardment Ion Thrusters," in *Advances in Electronics and Electron Physics*, Vol. 36, p. 265-373, Academic Press, 1974.
21. P. Wilbur, monthly report to the Jet Propulsion Laboratory, June 21, 2002.
22. Aston, G., Kaufman, H.R., and Wilbur, P.J., "Ion Beam Divergence Characteristics of Two-Grid Accelerator Systems," *AIAA Journal*, Vol.16, No. 5, 516-524, May 1978.